GEOLOGICAL SURVEY OF CANADA
OPEN FILE 7852

Targeted Geoscience Initiative 4: Contributions to the Understanding of Precambrian Lode Gold Deposits and Implications for Exploration

The Archean Côté Gold intrusion-related Au(-Cu) deposit, Ontario: A large-tonnage, low-grade deposit centred on a magmatic-hydrothermal breccia

Laura R. Katz[1], Daniel J. Kontak[1], Benoît Dubé[2], and Vicki J. McNicoll[3]

[1]Laurentian University, Sudbury, Ontario
[2]Geological Survey of Canada, Québec, Quebec
[3]Geological Survey of Canada, Ottawa, Ontario

2015

Recommended citation

Katz, L.R., Kontak, D.J., Dubé, B., and McNicoll, V.J., 2015. The Archean Côté Gold intrusion-related Au(-Cu) deposit, Ontario: A large-tonnage, low-grade deposit centred on a magmatic-hydrothermal breccia, *In:* Targeted Geoscience Initiative 4: Contributions to the Understanding of Precambrian Lode Gold Deposits and Implications for Exploration, (ed.) B. Dubé and P. Mercier-Langevin; Geological Survey of Canada, Open File 7852, p. 139–155.

Publications in this series have not been edited; they are released as submitted by the author.

Contribution to the Geological Survey of Canada's Targeted Geoscience Initiative 4 (TGI-4) Program (2010–2015)

TABLE OF CONTENTS

The Archean Côté Gold intrusion-related Au(-Cu) deposit, Ontario: A large-tonnage, low-grade deposit centred on a magmatic-hydrothermal breccia

Laura R. Katz[1]*, Daniel J. Kontak[1], Benoît Dubé[2], and Vicki J. McNicoll[3]

[1]Department of Earth Sciences, Laurentian University, Sudbury, Ontario P3E 2C6
[2]Geological Survey of Canada, 490 rue de la Couronne, Québec, Quebec G1K 9A9
[3]Geological Survey of Canada, 601 Booth Street, Ottawa, Ontario K1A 0E8
*Corresponding author's e-mail: lkatz@laurentian.ca

ABSTRACT

The recently discovered Côté Gold deposit, located in the southeast limb of the Swayze greenstone belt, Abitibi Subprovince, is an Archean low-grade, high-tonnage Au(-Cu) deposit. The deposit is hosted by the 2741 Ma Chester intrusive complex (CIC), a high-level, multi-phase, laccolithic-shaped synvolcanic intrusion composed of several tonalite and diorite phases. Although a close temporal and spatial relationship exists between the phases of the CIC, whole-rock geochemistry on least-altered samples suggests they are petrogenetically unrelated. Notably, the tonalite phases are characterized chemically as low-Al type, which is atypical of the tonalite-trondhjemite-granodiorite suites in the Archean Superior Province and elsewhere, but typical of primitive arc submarine environments. The mineralized system at the Côté Gold deposit is co-spatial with a multi-phase, magmatic-hydrothermal breccia body that contains multiple brecciation events and matrices and is overprinted by several alteration types (biotite, sericite, silica-sodic). Whole-rock geochemistry indicates that the deposit is Au(-Cu) only and is relatively depleted in other elements (e.g. As, F, Bi, Te). The overlap of Re-Os dates on syn-gold-deposition molybdenite (2739 ± 9 Ma) with the 2741 Ma CIC is consistent with field observations that suggest an overlap of magmatic and hydrothermal events. The results of this study have defined a new significant early stage gold metallogenic event in the Abitibi Subprovince at 2740 Ma and the deposit provides a guide for future exploration in other composite, subvolcanic, low-Al intrusions in the Archean.

INTRODUCTION

The recently discovered (2009/2010) Côté Gold deposit, located in the Archean Swayze greenstone belt, Abitibi Subprovince of northern Ontario, is a large-tonnage, low-grade Au(-Cu) deposit with an indicated resource of 269 Mt averaging 0.88 g/t Au (7.61 M oz) and an inferred resource of 44 Mt averaging 0.74 g/t Au (1.04 M oz) at a 0.3 g/t Au cut-off grade (IAMGOLD, 2013). The discovery of the Côté Gold deposit initiated a deposit-scale study that was undertaken as part of the Discover Abitibi Initiative. This study provided the first description of the host rocks and related alteration types and mineralization, whole-rock and alteration geochemistry, stable isotope geochemistry and U-Pb and Re-Os geochronology (Kontak et al., 2013). Two U-Pb zircon samples yielded ages of 2741.1 ± 0.9 and 2738.7 ± 0.8 Ma for a tonalite and tonalite breccia, respectively, which overlaps with two Re-Os molybdenite dates (avg. 2739 ± 9 Ma), one sample of which contained coarse gold. The significance of this discovery and initial study resulted in further studies, which included Ph.D. and M.Sc. theses that focused on a full characterization of the deposit and a structural synthesis of the ore system and surrounding area. The work is supported financially and logistically through Iamgold Corporation with funding for a comprehensive lithogeochemical and U-Pb geochronological study funded from Geological Survey of Canada through the TGI-4 Lode Gold Project. This article focuses on the aspects of the project associated with the TGI-4 mandate and therefore includes a general description of host rocks, nature and style of alteration and mineralization, U-Pb zircon geochronology, and geochemistry.

RESULTS AND DATA ANALYSIS

Geology of the Côté Gold Deposit

The Au(-Cu) Côté Gold deposit is located in the southern limb of the Swayze greenstone belt (SGB), part of the gold-rich Abitibi Subprovince (Fig. 1). The SGB

Katz, L.R., Kontak, D.J., Dubé, B., and McNicoll, V.J., 2015. The Archean Côté Gold intrusion-related Au(-Cu) deposit, Ontario: A large-tonnage, low-grade deposit centred on a magmatic-hydrothermal breccia, *In:* Targeted Geoscience Initiative 4: Contributions to the Understanding of Precambrian Lode Gold Deposits and Implications for Exploration, (ed.) B. Dubé and P. Mercier-Langevin; Geological Survey of Canada, Open File 7852, p. 139–155.

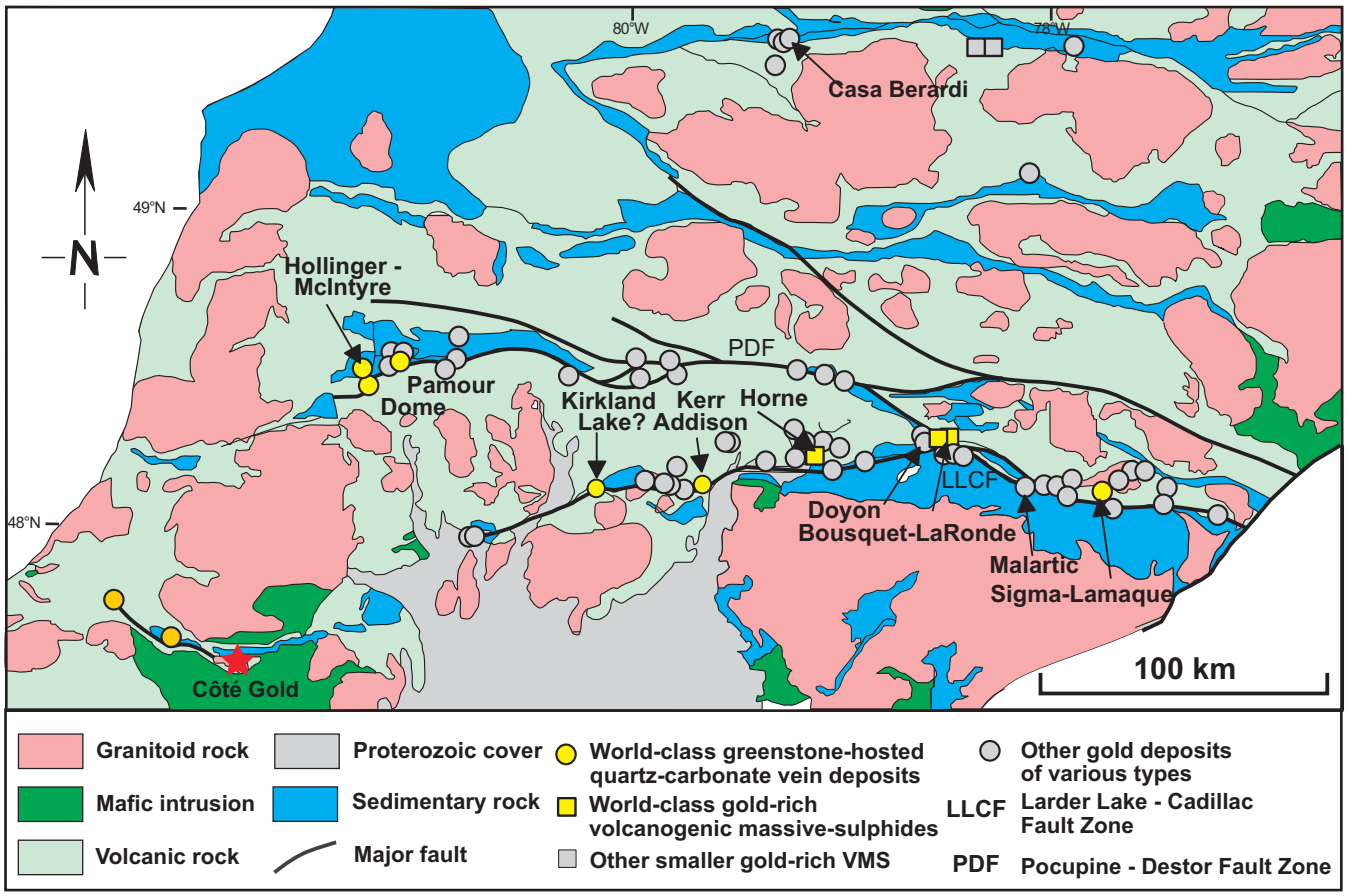

Figure 1. Simplified geological map of the Abitibi Subprovince showing the major gold deposits and fault zones. Red star shows the location of the Côté Gold deposit. Modified from Dubé and Gosselin (2007) and Poulson et al. (2000).

(2750–2670 Ma) contains many of the stratigraphic assemblages and structures typical of the southern Abitibi greenstone belt (AGB) based on lithology and geochronology criteria (Ayer et al., 2002; van Breemen et al., 2006). Several, regionally extensive, D_2 (ca. 2697–2675 Ma) high-strain zones transect the SGB. The D_2 deformation in the SGB, like in the AGB, is inferred to have been synchronous with the generation of orogenic style gold mineralization (Heather, 2001; van Breemen et al., 2006). Metamorphic grade within the southern Abitibi greenstone belt ranges from subgreenschist to greenschist. Peak metamorphism is estimated to have occurred from 2677 to 2643 Ma (Powell et al., 1995).

The deposit is hosted by the ca. 2741 Ma Chester intrusive complex (CIC), a multi-phase, locally layered, laccolithic-shaped, synvolcanic intrusion composed of tonalite and diorite (Fig. 2). The deposit is centred on a magmatic-hydrothermal breccia body that intrudes tonalitic and dioritic rocks.

The CIC intruded into the mafic volcanic rocks of the Arbutus Formation, which forms the basal formation in the Chester Group. The formation consists of low-K tholeiitic pillow basalts, mafic flows, and sills.

The Yeo Formation forms the upper formation in the Chester Group and overlies the CIC (Fig. 2). The Yeo Formation consists of intercalated felsic and intermediate volcanic rocks, clastic sedimentary and volcaniclastic rocks, iron formation and Fe-rich sedimentary rocks. The felsic and intermediate volcanic rocks range from poorly sorted to well bedded, monolithic and heterolithic lapilli to volcanic breccia tuffs, feldspar crystal ash tuffs, massive aphanitic flows and feldspar ± quartz phyric flows (Heather, 2001). Three previous U-Pb zircon dates were obtained from felsic lapilli tuffs at 2739 ± 2 and 2734 ± 2 Ma (Heather and Shore, 1999a,b), and 2739 ± 1 Ma (van Breemen et al., 2006; Fig. 2). Previous geochemical studies have interpreted the Yeo Formation to be the eruptive equivalent of the CIC (Heather et al., 1996; Berger, 2012).

The Chester Group is equivalent to the Pacaud Assemblage in the Abitibi greenstone belt. The Chester Group is inferred to have both ensimatic ocean basin and arc signatures (Ayer et al., 2002; van Breemen et al., 2006).

Host Rocks

The deposit is hosted by several phases of tonalite and diorite sills that display complex cross-cutting relation-

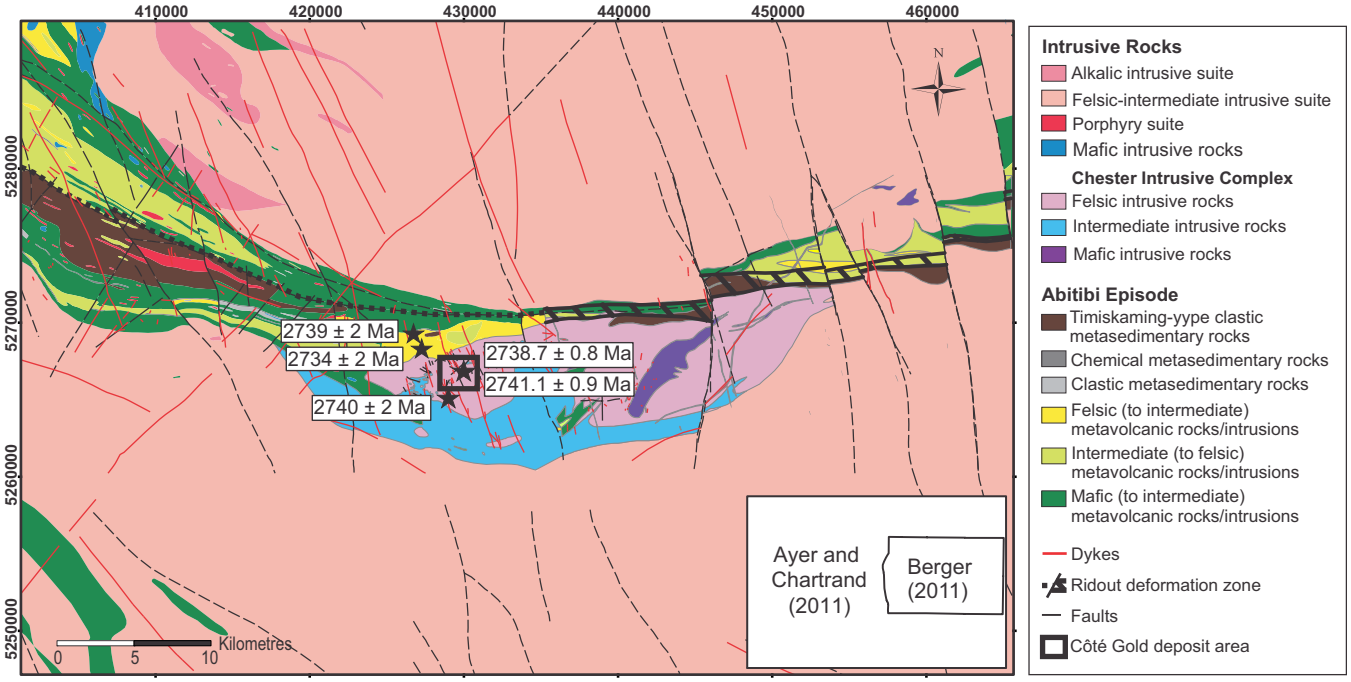

Figure 2. Simplified district-scale geological map of the Chester intrusive complex and the southeastern arm of the Swayze greenstone belt, compiled from Ayer and Chartrand (2011) and Berger (2011). Deposit area is shown in the black box. Location of previous geochronology dates are shown by black stars.

ships. Based on their relative timing and variable chemistry, five distinctive intrusive phases have been identified: (1) tonalite I; (2) diorite; (3) aphyric to quartz and/or plagioclase porphyritic quartz diorite; (4) tonalite II; and (5) hornblende-plagioclase ± quartz pegmatite. The Côté Gold deposit is centred on a mineralized magmatic-hydrothermal breccia body that intrudes tonalite and diorite rocks (Fig. 3a, c). Drill-core logging and detailed mapping of select exposures (e.g. North Breccia outcrop; Fig. 4) have established the basis for the relative timing of intrusive phases and the current nomenclature presented below.

Tonalite I, which forms sills with 10s to 100s of metres of apparent thickness, is a light grey, massive, equigranular rock composed of fine- to medium-grained plagioclase and quartz (Fig. 5a), with rare plagioclase or quartz phenocrysts. Accessory minerals include titanite, zircon, apatite, rutile, ilmenite, tourmaline, monazite, and xenotime. This unit has a hypidiomorphic granular texture with rare development of granophyre (Fig. 5b) and miarolitic cavities (Fig. 5c). Plagioclase has oscillatory zoning, polysynthetic twinning and rarely sieve textures. Miarolitic-like cavities include quartz ± sulphide, quartz-chlorite and quartz-plagioclase types that are typically oblate in shape and range from <5 mm to 10s of cm in diameter.

The diorite phase comprises sills of 5 to <150 metres in apparent thickness that intrude tonalite I and can be exhibit chilled margins. The contact between the diorite and tonalite I is commonly brecciated and, where this occurs, is termed a magmatic breccia with tonalite clasts in a dioritic matrix. The diorite is dark-green, massive to rarely foliated, equigranular to inequigranular and medium- to coarse-grained (Fig. 5d). The diorite contains variable amounts of plagioclase, amphibole, titanite, magnetite and ilmenite with accessory apatite, zircon, and tourmaline. This unit rarely has a granophyric texture and plagioclase shows primary oscillatory zoning and polysynthetic twinning.

Aphyric to quartz and/or plagioclase porphyritic quartz diorite consists of sills that range from 5 to <150 m in apparent thickness and intrudes into diorite. Quartz diorite is dark- to light-green, inequigranular, medium- to coarse-grained and is massive; locally it contains quartz phenocryst and rarely porphyritic plagioclase (Fig. 5e). The unit consists of plagioclase, amphibole, quartz, titanite, magnetite and ilmenite with accessory apatite, zircon, and tourmaline. The plagioclase contains primary oscillatory zoning, polysynthetic twinning and granophyric texture occurs.

The contact relationships of diorite and quartz diorite phases are variable, with both sharp and diffuse contacts. In both cases, diorite or quartz diorite clasts are present along the contact which gives a breccia texture whereby the more leucocratic quartz diorite matrix host melanocratic diorite clasts (Fig. 5e). This commonly observed cross cutting relationship suggests that diorite evolved over time, fractionating to more leucocratic quartz diorite.

Tonalite II forms sills of a few metres to 100s of metres in apparent thickness and is mineralogically and

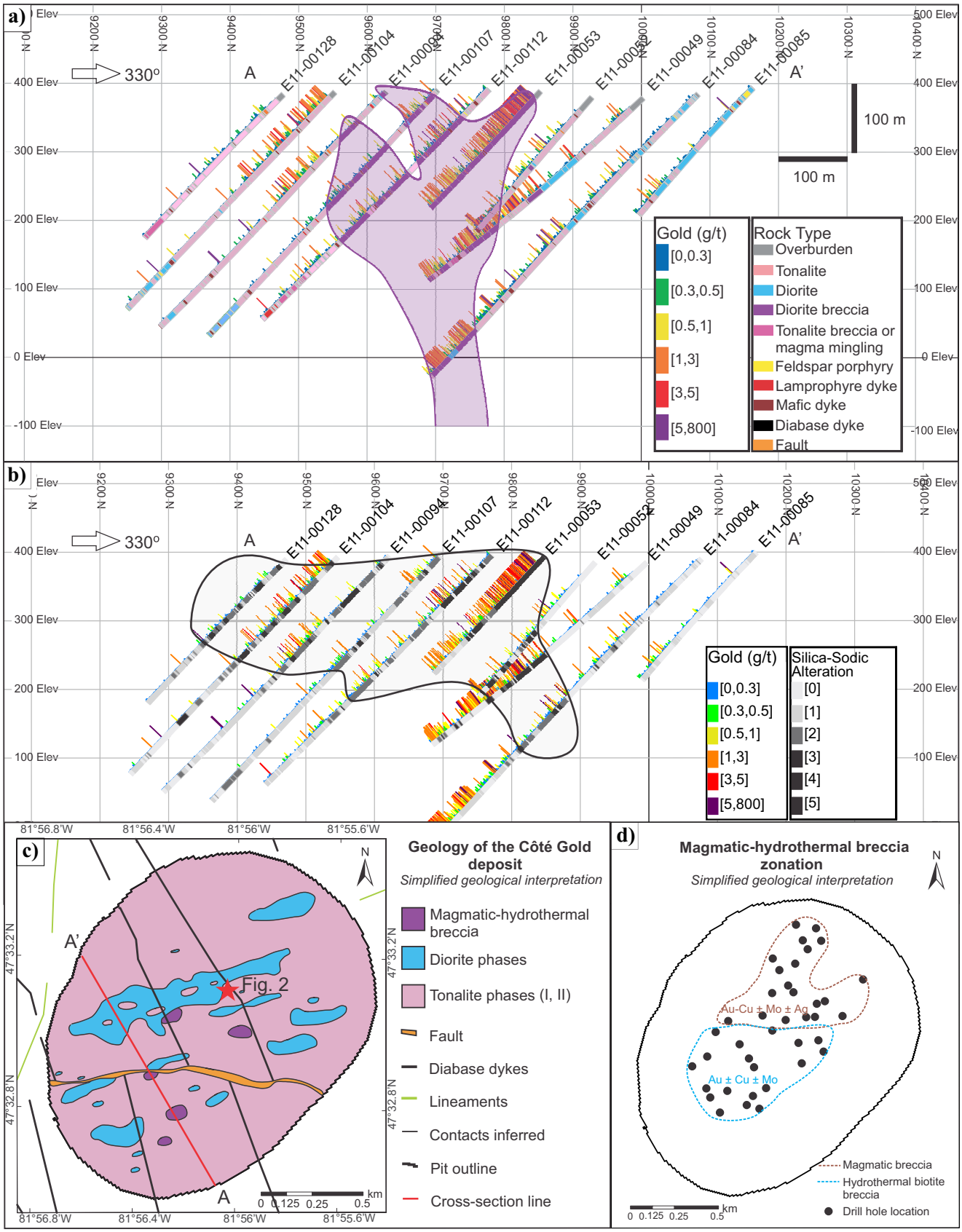

Figure 3 opposite page. a) Cross section of line 87+00 through the Côté Gold deposit showing the distribution of rock types. **b)** Extent of silica-sodic alteration. **c)** Plan-view map inside the proposed open pit. The location of cross-section A-A' is indicated by the red line and the location of the North Breccia outcrop (Fig. 4) is indicated by the star. Map was created using the first bedrock geology from 373 drillholes. **d)** Schematic plan view map of breccia matrix zonation and associated metals.

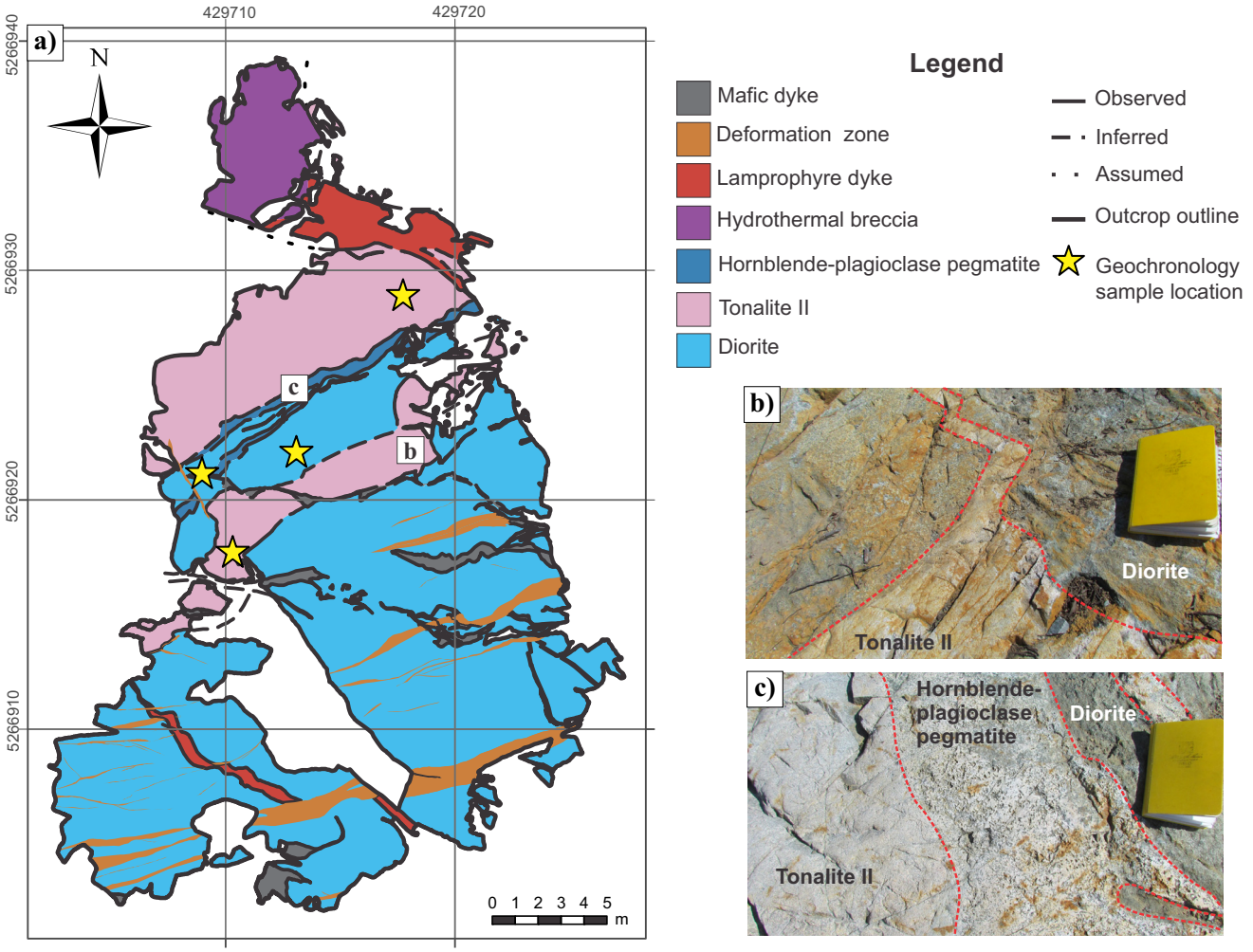

Figure 4. a) Geological map of the North Breccia outcrop showing the relative timing of the main geological units in the Côté Gold deposit. The locations of samples used for U-Pb zircon geochronology are indicated with stars. **b)** Field photograph of tonalite II cutting diorite. **c)** Field photograph showing the hornblende-plagioclase pegmatite intruding along the contact between the diorite and tonalite II. Book for scale is 19 x 12 cm.

texturally similar to tonalite I, but differs in terms of relative timing. The diorite and quartz diorite have sharp contacts with the older tonalite I phase and has transitional to sharp contacts with the younger tonalite II phase (Fig. 4b). The nature of the shape of the diorite clasts (millimetre- to metre-size; angular, rounded and scalloped contacts) in tonalite II suggests emplacement of tonalite II before the complete crystallization of dioritic phases.

Hornblende-plagioclase ± quartz pegmatite is the least abundant magmatic phase and generally occurs as small dykes of <1 m in apparent thickness. This unit is spatially associated with diorite and quartz diorite and has sharp to diffuse contacts with these phases (Fig. 4c). These pegmatitic dyke rocks are dark- to light-green, very coarse-grained (up to 2.5 cm) and inequigranular to massive. The mineralogy consists of plagioclase, hornblende, quartz, titanite, magnetite and apatite. Granophyric texture occurs and plagioclase is characterized by oscillatory zoning and polysynthetic twinning. This phase contains rare acicular amphibole grains (Fig. 5f).

Tonalite and diorite phases are intruded by a mineralized, sill-like magmatic-hydrothermal breccia body (~1200 m north-south and ~600 m east-west), on which the Au(-Cu) deposit is centred. The breccia body is complex, as both magmatic and hydrothermal variants occur as indicated by the nature of the matrix. Three types of matrices occur: (1) magmatic matrix with a dioritic mineralogy consisting of plagioclase-amphibole ± quartz (Fig. 5g) and rarely an evolved diorite consisting of quartz-plagioclase-biotite; (2) a rare amphibole-rich hydrothermal matrix consisting of amphibole-quartz ± biotite ± carbonate ± sulphides; and (3) a biotite-rich hydrothermal matrix. The biotite-rich breccia can be subdivided into three types based mainly on mineralogy and texture: (i) a biotite-quartz ± epidote ± carbonate ± pyrite ± chalcopyrite ± allanite ± magnetite, (ii) a biotite-quartz-magnetite-pyrite-chalcopyrite-carbonate ± allanite ± apatite, and a (iii)

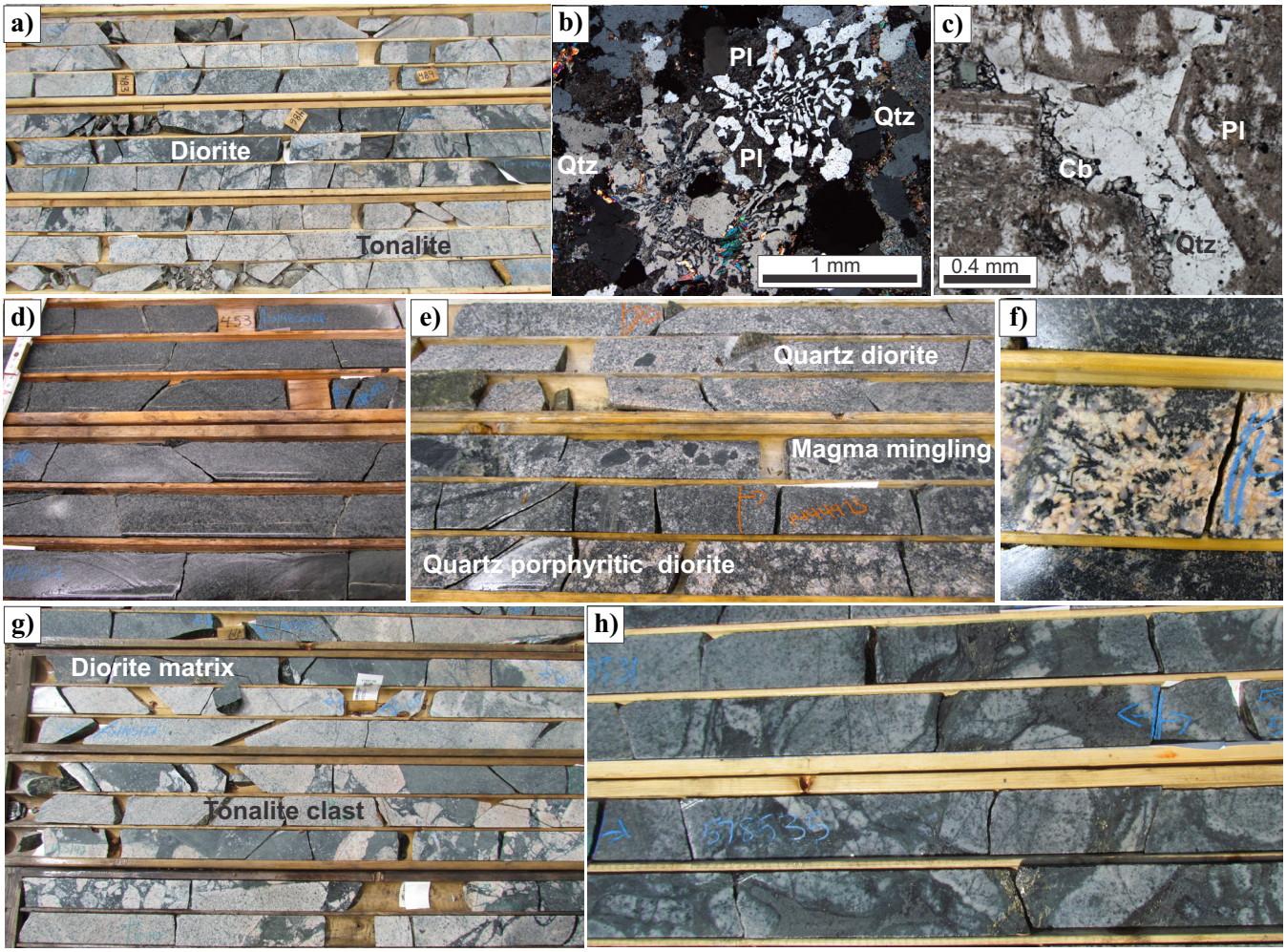

Figure 5. Drill-core and thin-section photographs showing the major rock types in the Côté Gold deposit. Width of drill core is 4.5 cm. **a)** Diorite intruding and brecciating (<5 m) tonalite I. **b)** Granophyric texture, which is common in the tonalite (Qtz = quartz, Pl = plagioclase). **c)** Miarolitic cavity in tonalite lined by carbonate (Cb) and filled with quartz. **d)** Section of homogeneous, medium-grained and equigranular melanocratic diorite. **e)** Contact between quartz diorite and quartz porphyritic diorite showing textural evidence for magma mingling. **f)** Hornblende-plagioclase-quartz pegmatite with acicular-textured amphibole grains. **g)** Section of magmatic breccia with tonalite clasts in a dioritic matrix. **h)** Section of biotite-rich hydrothermal matrix with clasts of tonalite.

biotite-quartz-carbonate-pyrite-chalcopyrite ± magnetite ± apatite (Fig. 5h).

The magmatic and biotite-rich hydrothermal breccia types can also be discriminated using geochemical parameters such as Zr/TiO_2 and CaO. The magmatic breccia is characterized by having relatively lower Zr/TiO_2 and elevated CaO values, thus similar to the chemistry of the diorite, whereas relatively higher Zr/TiO_2 and lower CaO values indicate a hydrothermal breccia. Using these indices (CaO and Zr/TiO_2), along with petrographic evidence, the data indicates an apparent zoning of breccia types exists in the deposit with the magmatic component occurring in the south and the biotite-rich hydrothermal breccia occurring in the north (Fig. 3d).

The division of breccia matrices in the deposit is also reflected in different metal associations, as illustrated in Figure 3d. The magmatic breccia is characterized by an Au ± Cu ± Mo association whereas the biotite-rich hydrothermal breccia is characterized by a Au-Cu ± Mo ± Ag association. There is, however, an overall lack of elemental associations in the Côté Gold deposit. Several bivariant elemental plots indicate there is no obvious correlation of Au mineralization with Cu, Mo, Te, F, Bi, or As in tonalite and diorite rocks (Fig. 6). However, in the breccia unit Au has a moderate positive correlation with Cu and Te, and a weak correlation with F.

The breccia body is characterized by the presence of tonalite I and II clasts. Rare dioritic clasts occur in the magmatic breccia. Tonalite, diorite, quartz diorite and hornblende-plagioclase pegmatite clasts are angular to rounded and variably sized, with dimensions from <1 mm to rarely >1 m in apparent length, and sharp to diffuse contacts. The breccia is typically matrix supported, but can rarely be clast-supported.

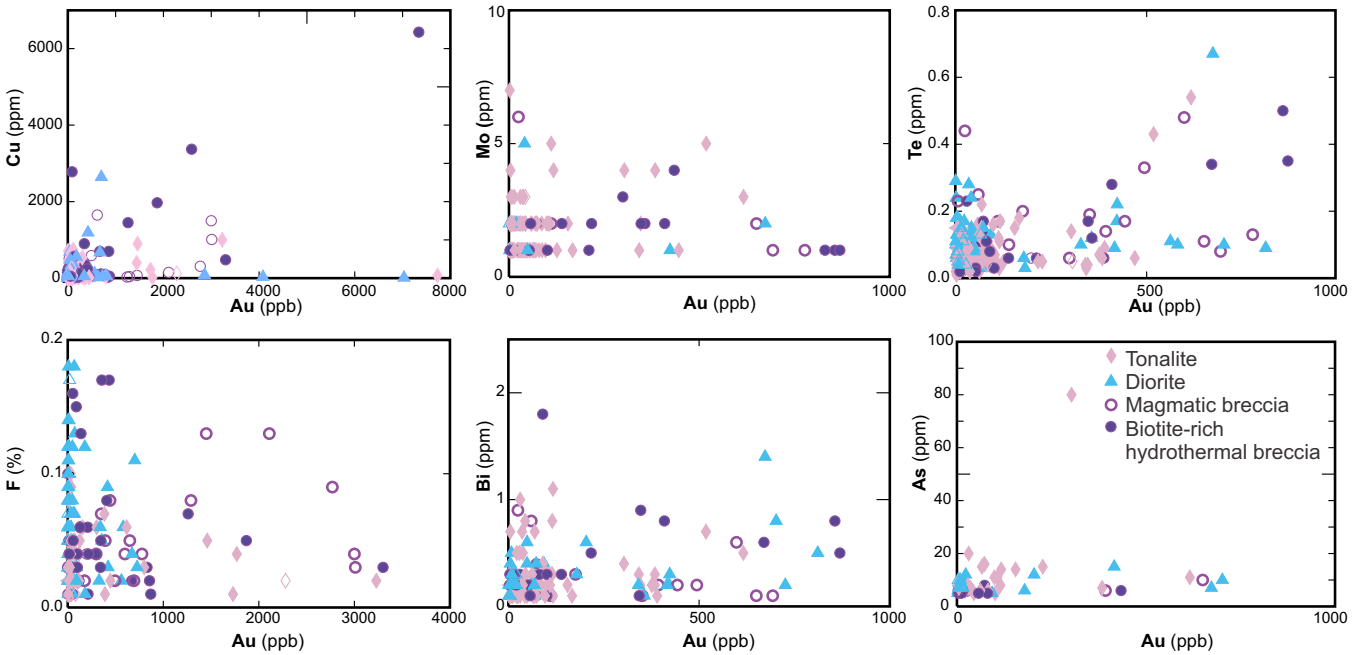

Figure 6. Binary element plots for all units in the Côté Gold deposit. The diagrams show that there is generally a poor correlation of all the elements with Au exception of the breccia unit where Au has a moderate association with Cu (correlation coefficient, R, of 0.76), moderate Au-Te association (R of 0.65) and weak Au-F association (R of 0.33).

Dyke Rocks

A variety of late, post-CIC dyke rocks cut the deposit. The dyke rocks are minor in total abundance and range in age from syn-SGB formation to post-deformation in age. Dyke rocks are not abundant in the deposit and are typically unmineralized. The dyke rocks include feldspar ± quartz porphyries, lamprophyre dykes and dioritic dykes, biotite-chlorite-quartz-carbonate dykes, diabase dykes, and tectonic breccias.

Geochemistry of Tonalitic and Dioritic Phases

A total of 455 samples were sampled to characterize the lithogeochemistry of the Côté Gold deposit. Included in the sample suite were major rock types, dykes, temporally-related volcanic rocks, as well as all alteration types and mineralization styles. Included in this summary herein are the least-altered tonalite and diorite samples. Table 1 presents a summary of analyses used in this study. The whole-rock geochemical data were obtained at Activation Laboratories, Ancaster, Ontario.

The intrusive rocks from the CIC are classified on the basis of their normative mineralogy (QAP) and the Zr/TiO_2 versus SiO_2 plot (Fig. 7a). In terms of their bulk compositions tonalite rocks equate to dacite and rhyolite. Some of the tonalite samples are notably enriched in silica (>74% SiO_2; Fig. 7a). The tonalite samples equate to the low-Al type (<15 wt% Al_2O_3) based on their Al_2O_3 contents at 70 wt% SiO_2 (Fig. 7b; Barker, 1979). This is atypical for these rocks, as the majority of Archean TTG are of high-Al type (>15 wt% Al_2O_3). The tonalite phases of the CIC have a range in terms of their Zr/Y versus Y ratios which equates to FII or FIIIa rhyolites (Fig. 7c). Importantly, the FII- and FIII-type rhyolites have been noted to be prospective for volcanic associated base-metal mineralization (Lesher et al., 1986). Tonalite samples contain a calc-alkaline to transitional affinity (Fig. 7d), with one tonalite sample plotting in the tholeiitic field.

The least-altered tonalite I and II are both characterized by relatively flat REE patterns with low (La/Yb)N ratios (Fig. 7e) and have moderate negative Eu anomalies (EuN/Eu*) of 0.30 to 0.77 and 0.27 to 0.63, respectively. In multi-element mantle-normalized plots tonalite I and II display similar patterns. Tonalite I and II display strong negative Ti, Eu P, Sr, with moderate Nb and Ta with variably negative Rb and Ba anomalies and positive Zr and Pb anomalies (Fig. 7f). The pronounced negative Eu anomalies and low Sr contents for both tonalite phases indicate plagioclase-dominated fractionation. On average, higher Ba, Sr and Ti occurs in tonalite II, which may be due to the presence of diorite clasts which are absent in tonalite I. These diorite clasts were originally amphibole-rich, but amphibole can be altered to biotite (Fig. 7f).

The diorite samples plot in the basalt to andesite field and quartz diorite samples plot in the andesite to dacite field in the Zr/TiO_2 versus SiO_2 plot (Fig. 7a). In terms of their normative mineralogy the quartz diorite phases rarely extend into the tonalite field as hornblende tonalites (Fig. 7a). Diorite is tholeiitic in nature and quartz diorite is tholeiitic to transitional in nature

Table 1. Average compositions of least altered major rocks from the Chester intrusive complex.

Rock Type	Tonalite I			Diorite			Tonalite II		
	Avg	STD	No.	Avg	STD	No.	Avg	STD	No.
SiO_2	77.07	2.56	6	56.11	5.53	15	71.87	2.55	6
Al_2O_3	11.94	0.62	6	14.91	1.09	15	13.39	1.00	6
Fe_2O_3	0.25	0.23	5	1.93	0.87	15	0.77	0.48	5
FeO_T	0.22	0.21	5	1.74	0.78	15	0.69	0.43	5
MnO	0.01	0.01	6	0.12	0.04	15	0.03	0.01	6
MgO	0.40	0.47	6	3.87	1.48	15	0.85	0.33	6
CaO	1.87	0.95	6	7.98	1.71	15	2.69	0.68	6
Na_2O	5.19	0.69	6	3.84	0.52	15	4.97	0.96	6
K_2O	0.60	0.14	6	0.66	0.46	15	0.98	0.41	6
TiO_2	0.315	0.017	6	1.489	0.471	15	0.532	0.311	6
P_2O_5	0.05	0.00	3	0.31	0.23	15	0.07	0.03	6
LOI	1.45	0.75	6	2.29	0.94	15	1.45	0.42	6
Total	99.97	0.67	6	100.19	0.53	15	99.47	0.79	6
Total S	0.08	0.06	5	0.07	0.10	14	0.05	0.04	5
CO_2	0.85	0.51	6	0.80	0.60	15	0.63	0.38	6
Cs	0.2	0.0	4	0.6	0.9	11	0.5	0.4	6
Rb	16	5	6	22	24	15	33	14	6
Ba	119	64	6	114	83	15	272	175	6
Th	7.93	2.64	6	2.68	1.21	15	7.35	2.36	6
U	1.80	0.33	6	0.94	0.64	15	1.85	0.44	6
Nb	7.1	2.0	6	9.1	4.0	15	12.1	7.0	6
Ta	0.85	0.16	6	0.75	0.73	15	0.89	0.09	6
Pb	7	1	2	3	2	9	3	1	5
Sr	103	43	6	254	72	15	160	76	6
Zr	269	32	6	141	51	15	259	46	6
Y	27.1	5.1	6	41.1	15.6	15	43.4	24.4	6
La	4.87	1.97	6	19.57	8.24	15	12.83	3.91	6
Ce	14.32	5.23	6	55.58	23.18	15	9.15	11.24	6
Pr	2.36	0.84	6	8.22	3.49	15	5.07	2.02	6
Nd	11.69	4.22	6	35.58	14.45	15	22.96	10.59	6
Sm	3.75	1.26	6	8.12	3.04	15	0.8	3.15	6
Eu	0.66	0.32	6	1.76	0.64	15	0.19	0.21	6
Gd	4.43	1.28	6	7.81	2.88	15	6.72	3.42	6
Tb	0.81	0.23	6	1.27	0.45	15	1.23	0.71	6
Dy	4.96	1.25	6	7.61	2.70	15	7.73	4.57	6
Ho	1.02	0.23	6	1.49	0.53	15	1.55	0.91	6
Er	3.10	0.68	6	4.33	1.45	15	4.65	2.65	6
Tm	0.49	0.10	6	0.65	0.22	15	0.74	0.43	6
Yb	3.21	0.57	6	4.22	1.43	15	4.72	2.7	6
Lu	0.437	0.060	6	0.605	0.196	15	0.647	0.355	6

Major elements as oxides in wt%, trace in ppm; Avg = average

(Fig. 7d). Both diorite and quartz diorite differ from a transitional to calc-alkaline nature for the tonalite samples.

The least altered diorite and quartz diorite have listric- or concave-shaped downwards LREE profiles with low La/YbN ratios and display weak negative Eu anomalies (EuN/Eu* = 0.43 to 0.89; Fig. 7g), hence they contrast markedly with the REE patterns for the tonalites. The multi-element mantle-normalized patterns for diorite and quartz diorite show weak negative Ti and Zr, moderate Rb, Ba, Nb, Ta, K, Sr, P anomalies and weak positive Pb anomalies (Fig. 7h). The mantle-normalized patterns for diorite differ from tonalite, the most obvious being the opposing Zr anomalies.

Post-Emplacement Veining and Alteration

Several types of magmatic-hydrothermal alteration are spatially associated with mineralization at the Côté Gold deposit. In paragenetic sequence, the dominant minerals associated to these alterations are amphibole, biotite, sericite, quartz-albite, epidote and chlorite (after biotite).

Amphibole alteration is rare in the deposit and occurs as a variety of amphibole-rich veins and breccias. Amphibole-bearing veins include amphibole, amphibole-quartz, amphibole ± apatite ± ilmenite ± titanite ± pyrite ± chalcopyrite assemblages (Fig. 8a). These veins cross cut the tonalite, diorite and the magmatic breccia and, therefore, post-date magmatic events. These amphibole-rich veins appear to be spatially restricted to the south of the deposit and represent the earliest hydrothermal alteration type associated with Au mineralization.

Biotite alteration is ubiquitous throughout the deposit and alters all intrusive phases. The biotite assemblage consists of biotite ± quartz ± magnetite ± epidote ± allanite ± carbonate ± pyrite ± chalcopyrite ± pyrrhotite ± titanite. This alteration assemblage occurs in the biotite-rich hydrothermal breccia (Fig. 8b), as disseminations in tonalite and diorite (Fig. 8c), in stockwork zones (Fig. 8d) and in sheeted veins (Fig. 8e). The biotite in the matrix of the biotite-rich hydrothermal breccia is not the result of alteration, but

Figure 7 (opposite page). Whole-rock geochemistry of least altered samples of tonalitic and dioritic phases of the Chester intrusive complex. **a)** A Zr/TiO_2 versus SiO_2 plot (Winchester and Floyd, 1975) for samples of diorite and tonalite, which was used to classify them chemically. Abbreviations: Alk-Bas = alkaline basalt, Bas/Trach/Neph = basanite/trachytes/nephelinite, Com/Pan = comendite/pantellite, Sub-AB = subalkaline basalt. The inset diagram shows the same samples plotted in the quartz-alkali feldspar-plagioclase (QAP) rock classification scheme. The pink shaded area shows tonalitic samples and the blue shaded area shows dioritic samples. Abbreviations: TT = tonalite-trondhjemite field and D = diorite/gabbro and quartz diorite/gabbro field. **b)** Plot of SiO_2 versus Al_2O_3 with the fields after Barker (1979) showing that the tonalite conforms to the low-Al type. **c)** Samples of tonalite plotted in the Y versus Zr/Y diagram, which shows their FII or FIIIa affinity. **d)** Samples of tonalite, diorite, and quartz diorite plotted on a Y versus Zr diagram; the fields for different magma associations from Galley and Lafrance (2014). **e)** Chondrite-normalized REE plot for samples of tonalite I and II. **f)** Multi-element mantle-normalized diagram for samples of tonalite I and II. **g)** Chondrite-normalized REE plot for samples of diorite and quartz diorite. **h)** Multi-element mantle-normalized diagram for samples of the different diorite and quartz diorite. The CI chondrite normalizing and primitive mantle values used are from Sun and McDonough (1989).

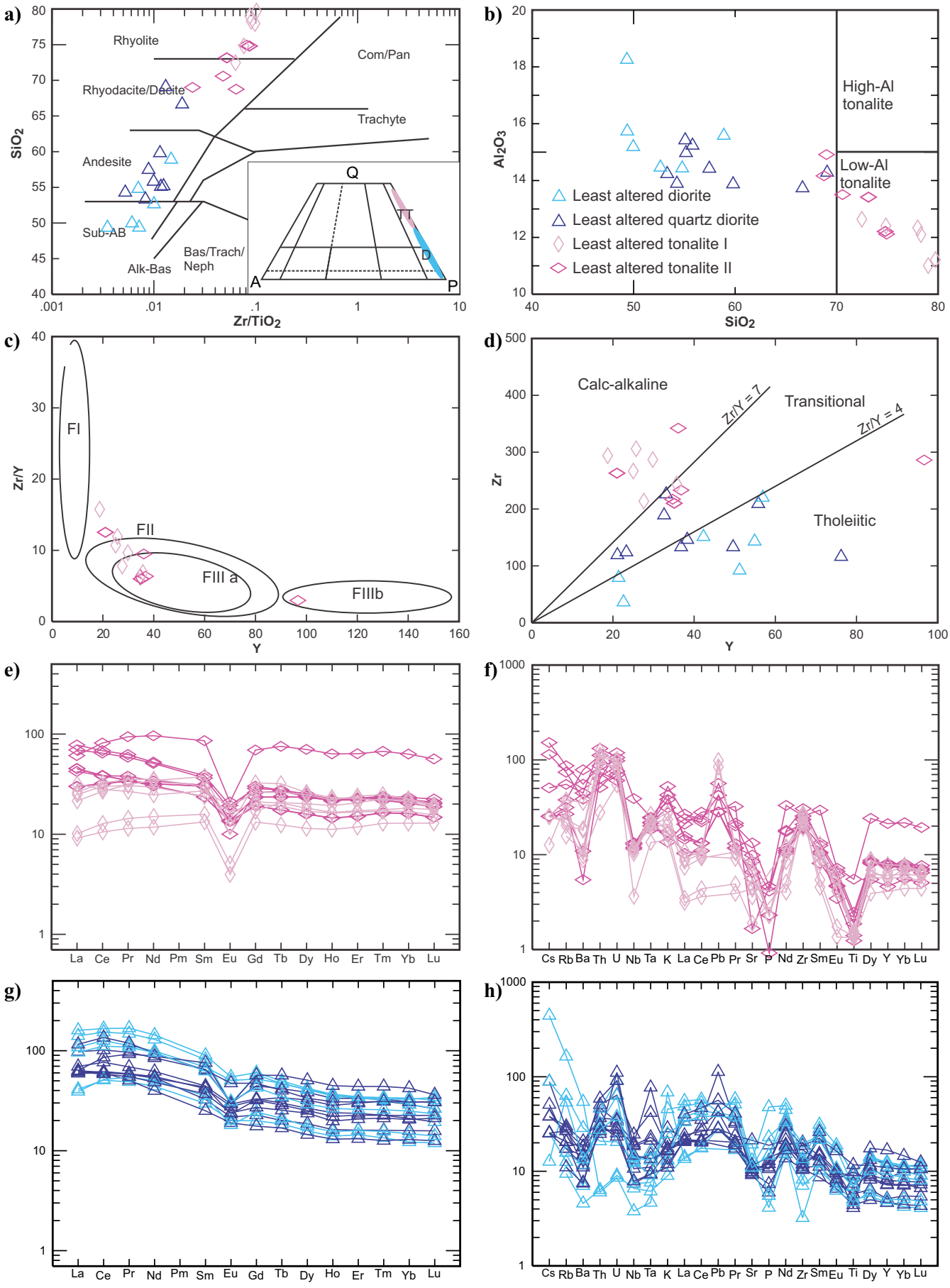
a)
Rhyolite
Com/Pan
Rhyodacite/Dacite
Trachyte
Andesite
Sub-AB
Alk-Bas
Bas/Trach/
Neph
Q
T
D
A
P
SiO2
Zr/TiO2
b)
High-Al
tonalite
Low-Al
tonalite
Least altered diorite
Least altered quartz diorite
Least altered tonalite I
Least altered tonalite II
Al2O3
SiO2
c)
FI
FII
FIII a
FIIIb
Zr/Y
Y
d)
Calc-alkaline
Transitional
Tholeiitic
Zr/Y = 7
Zr/Y = 4
Zr
Y
e)
La Ce Pr Nd Pm Sm Eu Gd Tb Dy Ho Er Tm Yb Lu
f)
Cs Rb Ba Th U Nb Ta K La Ce Pb Pr Sr P Nd Zr Sm Eu Ti Dy Y Yb Lu
g)
La Ce Pr Nd Pm Sm Eu Gd Tb Dy Ho Er Tm Yb Lu
h)
Cs Rb Ba Th U Nb Ta K La Ce Pb Pr Sr P Nd Zr Sm Eu Ti Dy Y Yb Lu

forms as a primary hydrothermal mineral. Disseminated biotite occurs as anhedral to subhedral, fine-grained (<1 to > 50%) disseminations that partly replace primary plagioclase and amphibole, as well as amphibole in veins and breccias. Sheeted veins consist of east-west trending, planar, subparallel, moderately to steeply dipping, closely (cm to 10s of cm apart) to widely (several metres apart) spaced veins that occur throughout the deposit. These veins are also found outside the deposit within the CIC. These sheeted veins contain quartz-biotite-pyrite ± chalcopyrite ± pyrrhotite ± carbonate ± titanite ± allanite and therefore inferred to be early, having formed during biotite alteration, but are typically overprinted by sericite alteration and deformation resulting in distinct sericite alteration haloes with or without shearing. The various types of biotite alteration noted above are partially to wholly altered by chlorite.

The sericite-bearing alteration assemblage consists of sericite-quartz ± carbonate ± pyrite ± chalcopyrite and occurs throughout the deposit. Sericite is light-grey to dark-grey and rarely green-grey with fine-grained, elongated to stubby grains that replace primary plagioclase. Sericite alteration is generally fracture-controlled as veins, disseminations and pervasive types. Sericite often forms alteration haloes surrounding stockworks (Fig. 8d) and sheeted veins (Fig. 8e,f), both of which contain an earlier biotite alteration assemblage. Although the extent of sericite alteration has not been fully determined, it is strongest within the centre of the deposit with its intensity decreasing with distance from the core of mineralization.

Silica-sodic alteration is a texturally-destructive alteration that occurs as vein-controlled (Fig. 8g) as well as a pervasive type that overprints earlier biotite and sericite alteration. The silica-sodic alteration envelope can be >200 m wide, moderately to steeply dipping to the north or northwest, and is most intensely developed towards the centre of the deposit. Figure 3b illustrates the distribution and intensity of the silica-sodic alteration, which also overprints the mineralized breccia body at depth. In drill core, the silica-sodic alteration is characterized by bleaching, destruction of primary textures, including grain boundaries, and replacement of mafic minerals. In thin section, this alteration is characterized by replacement of plagioclase by albite, grain-size reduction, and sutured grain boundaries due to dissolution of plagioclase and quartz. This alteration affects tonalite, diorite, quartz diorite, hornblende-plagioclase pegmatite, magmatic-hydrothermal breccia (Fig. 8h) and rarely dyke rocks. Gold mineralization can be spatially associated with this alteration (Fig. 8i), but it is typically inconsistent.

The epidote-bearing alteration, consisting of an epidote ± quartz ± carbonate ± chlorite assemblage, occurs as both disseminated and vein-controlled alteration (Fig. 8j). Epidote occurs as fine-grained anhedral disseminations in the groundmass replacing primary plagioclase and amphibole. An area of vein-controlled epidote alteration (Fig. 8j) is restricted to a ~300 m wide by 400 m long zone in the northern-most part of the deposit. Epidote alteration is rarely associated with Au mineralization. This alteration type appears to postdate the aforementioned alteration types based on limited crosscutting observations in drill core. This alteration is inferred to be syn-intrusion due to its spatial distribution in the deposit and that it is foliated, predating D_2 deformation.

Chlorite is ubiquitous throughout the deposit and occurs as disseminated, replacement and vein-controlled alteration. Petrographic observations indicate chlorite partially to wholly replace plagioclase, amphibole and secondary biotite. As a result of replacing biotite, titanium-bearing phases, such as rutile, form in association with chlorite. The timing of chlorite alteration is not fully constrained and therefore its importance in terms of deposit formation is unclear. Gold mineralization is spatially associated with hydrothermal chlorite alteration, but its genetic association is not fully understood as it pseudomorphs earlier, higher-temperature hydrothermal biotite.

The study and description of alteration types at the Côté Gold deposit is complicated by syn-tectonic alteration associated with regional D_2 deformation zones, including chlorite, sericite, silica, Fe- and Ca-carbonate, sulphidation and tourmaline alteration (Heather, 2001). At the deposit, syn-tectonic silica and sericite alteration are associated with D_2 deformation zones. Several discrete syn-tectonic shear zones, typically <3 m wide, cut through the deposit. Within the shear

Figure 8 (opposite page). Drill-core (width = 4.5 cm) and thin section photographs of alteration types and mineralization styles present at the Côté Gold deposit. **a)** Gold mineralized amphibole vein cutting through barren diorite. **b)** An example of mineralized, biotite-rich hydrothermal breccia with clasts of tonalite. **c)** Disseminated, light-brown to dark-brown, subhedral biotite (Bt) that replaces primary plagioclase (Pl) and more rarely quartz (Qtz). The opaque mineral is disseminated pyrite (Py). **d)** Stockwork developed in tonalite that is lined by biotite and quartz with sericite alteration haloes. **e)** Mineralized sheeted quartz-pyrite veins in tonalite. **f)** Close-up photograph of a multi-centimetre-thick quartz-pyrite-chalcopyrite-molybdenite vein with a sericite alteration halo in tonalite that forms part of a sheeted vein set. g) Example of fracture-controlled silica-sodic alteration overprinting disseminated and fracture-controlled biotite alteration. **h)** Example of the pervasive silica-sodic alteration of a breccia type of unknown magmatic or hydrothermal origin. **i)** An example of fracture-controlled silica-sodic alteration overprinting sericite alteration. j) An example of vein-controlled epidote alteration.

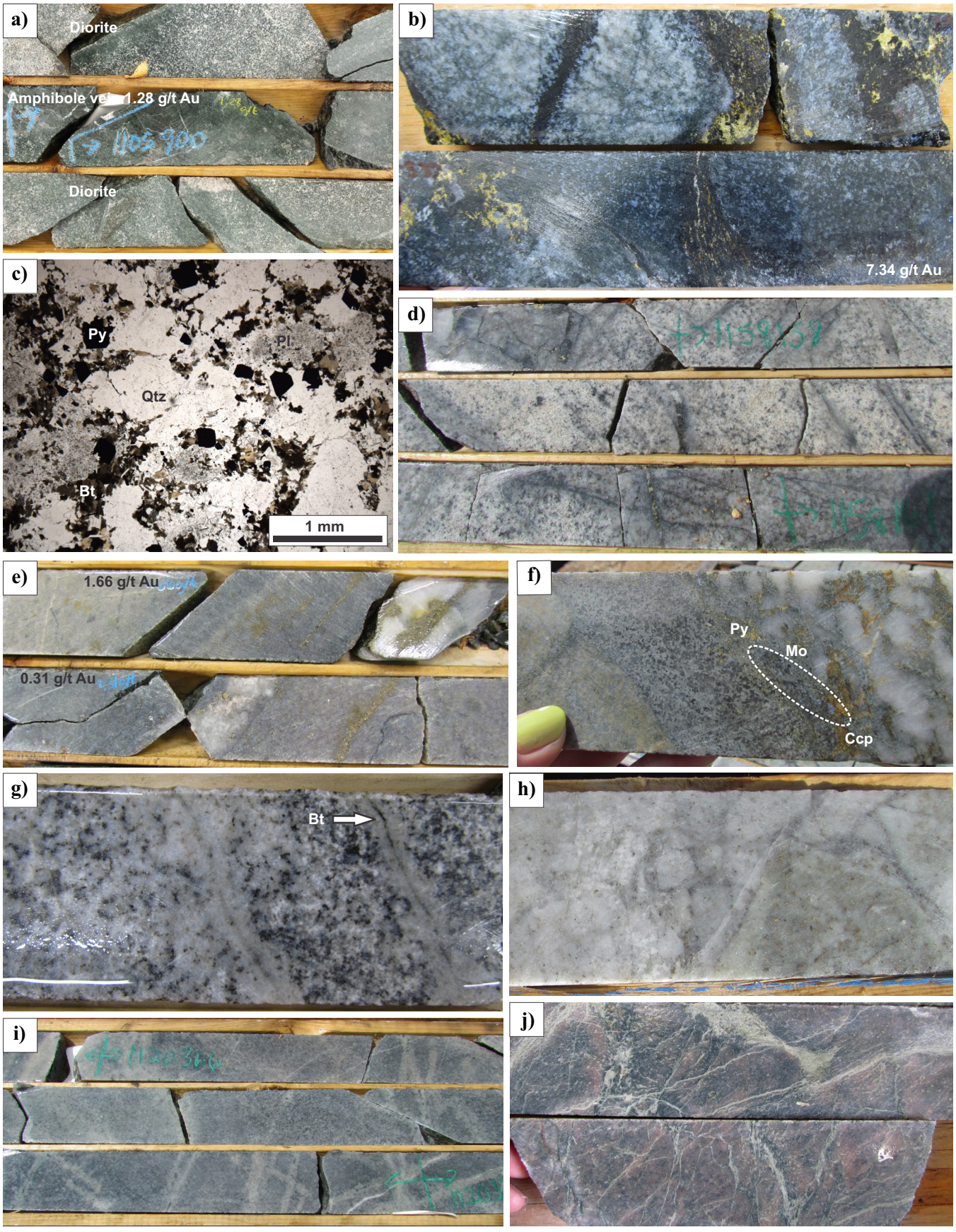
a)
Diorite
Amphibole ve
1.28 g/t Au
Diorite
b)
7.34 g/t Au
c)
Py
Pl
Qtz
Bt
1 mm
d)
e)
1.66 g/t Au
0.31 g/t Au
f)
Py
Mo
Ccp
g)
Bt
h)
i)
j)

zones there is the development of locally strong, pervasive sericite and silica alteration which overprints earlier syn-intrusion amphibole, biotite, sericite, silica-sodic and epidote alteration. Typically these shear zones do not contain mineralization. However, the shear zones can be mineralized when cutting through previously mineralized zones, such as a breccia unit or sheeted veins.

Mineralization

Several styles of Au mineralization are recognized within the Côté Gold deposit, and include disseminated, breccia-hosted and vein-type (Fig. 8). All of which are co-spatial with biotite (± chlorite), sericite and silica-sodic alteration.

Disseminated mineralization in the hydrothermal matrix of the breccia is the most important and consistent style of Au(-Cu) mineralization. This style consists of disseminated pyrite, chalcopyrite, magnetite, gold and molybdenite and is associated with primary hydrothermal biotite and chlorite after biotite (Fig. 8b). Similarly, disseminated mineralization in both tonalitic and dioritic rocks is associated with biotite or chlorite alteration (Fig. 8c). Although both biotite and chlorite are ubiquitous throughout the deposit, Au is not consistently associated with the two alteration types. Disseminated Au and chalcopyrite are intergrown with biotite/chlorite in the tonalite and breccia unit.

Several types and generations of veins host gold and molybdenite and include quartz, quartz-carbonate, quartz-biotite-pyrite ± chalcopyrite ± pyrrhotite ± carbonate ± titanite ± allanite, quartz-carbonate-titanite, quartz-tourmaline and quartz-epidote. The mineralized veins typically contain various proportions of pyrite and chalcopyrite. The nature of the veins and fractures vary from stockworks (Fig. 8d) to closely spaced, planar, subparallel sheeted vein sets (Fig. 8e, f). Stockwork mineralization cuts through all major rock types, but is most prominent in tonalite I and II versus the less competent dioritic unit. The mineralized sheeted veins and stockwork zones cut the hydrothermal breccia(s) and, therefore post-date the breccia-controlled mineralization. Miarolitic-like cavities, which consist of mm- to cm-size openings lined with feldspar, carbonate and sulphide, can also contain gold. Importantly, the gold-bearing sheeted and stockwork veins mineralization are not present in later post-CIC dykes suggesting a coeval syn-magmatic relationship.

Uranium-Lead Geochronology

The U-Pb zircon geochronology was done on four well-constrained samples collected from the North Breccia outcrop (Fig. 4 see location on Fig. 1c), and includes one diorite, two tonalites and one hornblende-plagioclase pegmatite. In addition, two feldspar-quartz porphyry dykes from drill core were sampled. Previous U-Pb zircon dating of tonalite I and II from the CIC includes 2740 ± 2 Ma (Heather and van Breemen, 1994; van Breemen et al., 2006; Fig. 2), 2741.1 ± 0.9 Ma, and 2738.7 ± 0.8 Ma (Kontak et al., 2013; Fig. 2).

Important field relationships mapped at the North Breccia outcrop are presented in Figure 4a–c. Diorite is the oldest rock type exposed and is intruded sharply by tonalite (Fig. 4b) that contains <1% dioritic clasts, which is characteristic of tonalite II. A hornblende-plagioclase pegmatite intrudes along the contact between diorite and tonalite II (Fig. 4c) and therefore postdates these phases. The results of the U-Pb zircon dating include (1) an age of 2741.5 ± 0.7 Ma for the diorite; (2) ages of 2741.7 ± 0.7 and 2741.4 ± 0.9 Ma for two tonalite samples; and (3) an age of 2741.0 ± 0.6 Ma for the pegmatite. The four samples constrain the age of crystallization of the CIC to 2741 Ma.

Two feldspar porphyry dykes that cross-cut mineralization were sampled to provide a minimum age for deposit formation. The first sample, an unaltered feldspar porphyry that cuts through a biotite altered tonalite (Fig. 9a), yielded an age of 2696.0 ± 0.9 Ma. The second sample, a sericite altered and deformed feldspar porphyry (Fig. 9b) cuts through a mineralized breccia unit, yielded a similar age of 2697.1 ± 0.8 Ma. These ages are among the youngest obtained for magmatic activity in the Swayze greenstone belt and do not constrain very well the minimum age for deposit formation.

Molybdenite Rhenium-Osmium Geochronology

Two samples previously analysed for molybdenite Re-Os dating were used to constrain the timing of mineralization (Kontak et al., 2013). The results yield ages of 2737 ± 11 Ma and 2741 ± 11 Ma for two tonalite-hosted samples, the former containing massive molybdenite in a fracture found in silica-sodic altered tonalite (Fig, 9c) and the latter containing visible molybdenite, chalcopyrite and gold in sericitized tonalite (Fig. 9d, e). Given that the two samples analysed yielded similar ages, the best estimate of the molybdenite Re-Os age is 2739 ± 9 Ma (Kontak et al., 2013). These two ages constrain the age of gold mineralization at the deposit.

DISCUSSION AND MODELS

Petrogenesis of Tonalite and Diorite

A previous geochemical study by Berger (2012) suggested that tonalite and diorite phases of the CIC are genetically related, however, geochemical evidence from this study suggests otherwise. The diorite contains slightly elevated LREE patterns compared to the less fractionated patterns and lower REE contents of tonalite. The less fractionated pattern of tonalite with moderate to strong negative Eu anomalies are inconsis-

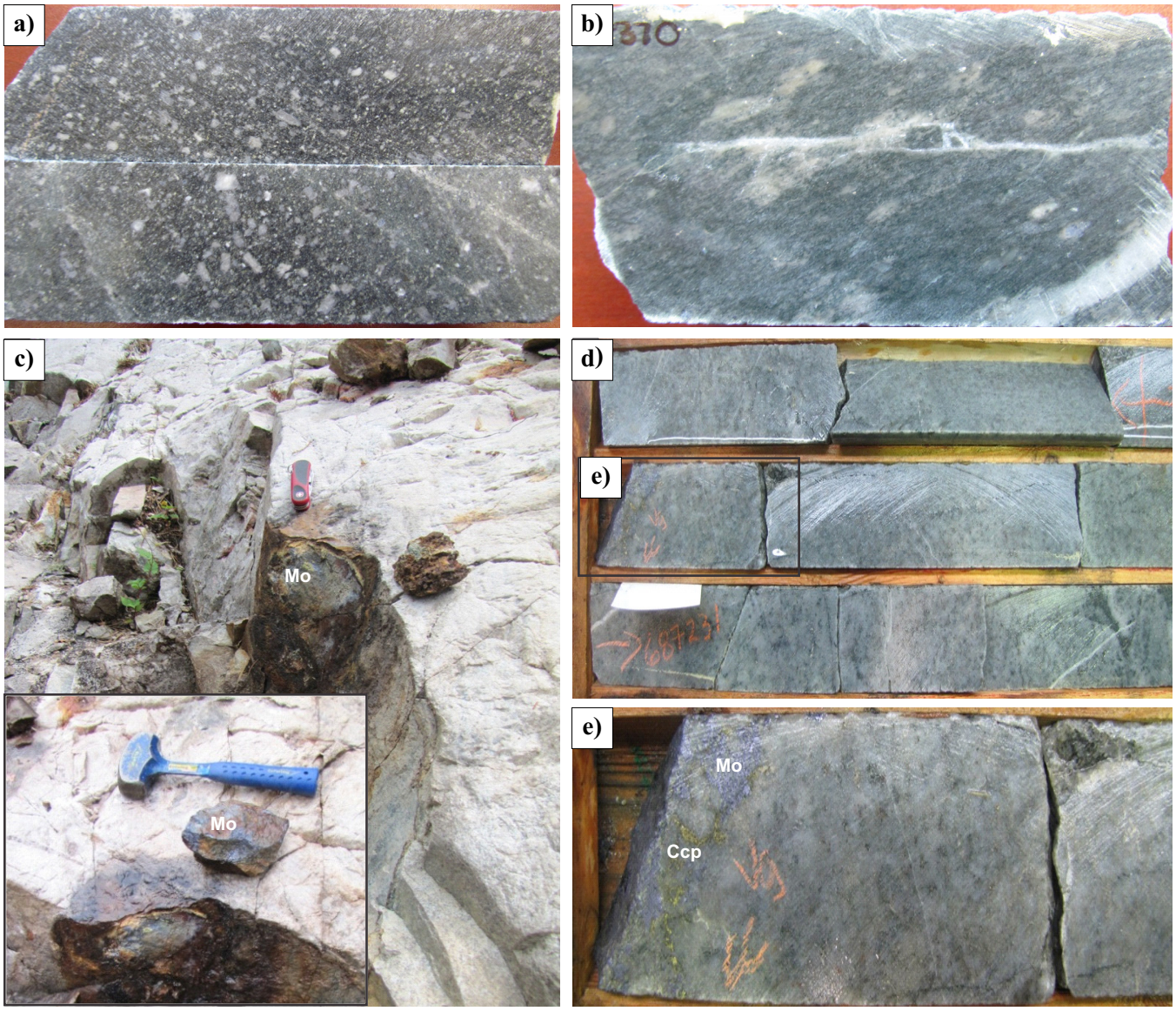

Figure 9. Field and drill-core (width = 4.5 cm) photographs of samples used for U-Pb and Re-Os geochronology. **a)** Unaltered feldspar porphyry. **b)** Sericite-altered and deformed feldspar porphyry dyke. **c)** Massive molybdenite (Mo) in a fracture in a silicified tonalite. In the inset, hammer for scale is 30 cm long. **d)** Molybdenite associated with chalcopyrite and gold in a veinlet cutting through a biotite altered tonalite that is overprinted by sericite alteration. **e)** Close-up photo of (d) showing molybdenite (Mo) intergrown with chalcopyrite (Ccp).

tent with being an evolved fractionate of the diorite, which is more elevated in the REEs and has a more fractionated pattern with a distinct listric- or concave-shaped downwards profile. Thus, although the tonalite and diorite are temporally related, this study suggests they are genetically unrelated.

The diorite and quartz diorite phases are tholeiitic to transitional in nature, whereas the tonalitic phases have a calc-alkaline to transitional affinity, based on their Zr/Y ratios. This spread of chemical affinity and, hence, petrogenetic associations for spatially associated rocks, in particular the quartz diorite-tonalite-trondhjemite suites, has been previously documented and could indicate that the intrusive suite consists of a composite of differentiated lithospheric mantle and lower-crust partial melts (Galley and Lafrance, 2014). Moreover, different petrogenetic associations is also supported by the differences in the primitive-mantle-normalized multi-element profiles between tonalite and diorite phases which suggests the involvement of two different magmas (i.e. mantle and crust; Galley, 2003). Both tonalite and diorite suites of the CIC display strong negative Ti, Eu P, and Sr, with moderate Nb and Ta, variably negative Rb and Ba anomalies, and positive Pb anomalies. The tonalite shows a decoupling between Nb and Zr which is typical of relatively reduced melts, whereas diorite shows a more sympathetic Nb/Zr decrease relative to primitive mantle, sug-

gesting a more evolved, oxidized source (Galley, 2003). This is consistent with petrographic evidence of accessory ilmenite in tonalite and accessory magnetite and ilmenite in diorite. The above evidence suggests a spread across petrogenetic origins for tonalitic and dioritic phases.

Metallogenic Implications

The known metallogenic events or epochs in the Abitibi greenstone belt were outlined by Robert (2001) and Robert et al. (2005) and occur in three main periods of gold mineralization which include (1) VMS from ca. 2728 to 2700 Ma; (2) syenite-associated from ca. 2680 to 2674 Ma; and (3) greenstone-hosted which spans from ca. 2671 to 2668 Ma. The U-Pb geochronology of this study constrains the intrusive phases of the CIC to ca. 2741 Ma which overlaps with the Re-Os dates of 2739 ± 9 Ma that constrain the age of molybdenite, some of which is associated with gold mineralization. These results, along with field and petrological evidence for syn-intrusion mineralization constrains the age of gold deposition. Therefore, at least some of the mineralization within the Côté Gold deposit defines a new and early-stage gold mineralization event within the Abitibi Subprovince. Possible later upgrading of this mineralization may have occurred due to structural overprinting, as has been documented at, for example, the Malartic intrusion-related gold deposit setting. This aspect of the Côté Gold deposit is being currently investigated given its significance for the deposit model.

IMPLICATIONS FOR EXPLORATION

Unlike the Abitibi greenstone belt that is rich in greenstone-hosted gold deposits, VMS, and syenite-associated gold deposits, few mineral deposits have been found so far in the SGB. Based on the similar geology of the two greenstone belts (Ayer et al., 2002), it seems reasonable to assume that the SGB should also be equally prospective for gold and base-metal deposits. Gold mineralization within the Abitibi Subprovince tends to be proximal to major faults, with the known deposits occurring in clusters (Dubé and Gosselin, 2007). Past exploration in the SGB focused on east-west trending, high-strain zones and greenstone-hosted quartz-carbonate vein-type deposits with minor success. The intrusion-related Côté Gold deposit is the first large gold deposit discovery in the SGB, and is similar to other low-Al composite suites described in the literature that have been documented to form in early arc rift environments that host VMS-style mineralization (Campbell et al., 1981; Galley, 2003). These subvolcanic, low-Al composite synvolcanic intrusions have also been documented to host porphyry-type Cu-Mo ± Au mineralization (Trowell 1974; Poulsen and Franklin, 1981; Galley, 2003). The Côté Gold deposit provides, therefore, a guide for future exploration activity for other low-Al composite, subvolcanic intrusive complexes within the SGB and other Archean terranes.

FUTURE WORK

The data reviewed here, which form part of a much more substantial data set, will be merged with other results and collectively assembled into three articles for submission to peer-reviewed journals. The tentative titles of each paper are as follows: (1) Geological setting, petrology and U-Pb zircon geochronology of an Archean large-tonnage, low-grade intrusion-related gold system: The Côté Gold Au(-Cu) deposit, Swayze greenstone belt, Ontario; (2) Mineral paragenesis, alteration and geochronology (U-Pb, Re-Os) of the Archean intrusion-related Côté Gold Au(-Cu) deposit, Ontario; and (3) Alteration lithogeochemistry of an Archean low-grade, large-tonnage intrusion-related gold deposit: The Côté Gold Au(-Cu) deposit, Swayze greenstone belt, Ontario.

ACKNOWLEDGEMENTS

This study is the outgrowth of support from several individuals and groups for which we are most appreciative. The initial work was supported by John Ayer and David Beilhartz and funded through Trelawney Mining and Exploration Inc. and the Discover Abitibi Program. Subsequently, Iamgold Corporation provided the considerable financial and logistical support needed to undertake this deposit-scale study and we sincerely acknowledge their financing and the input of staff, in particular Jamie Rogers, who made this project possible. We thank the financial support of the Geological Survey of Canada through the TGI-4 Lode Gold Project for providing funding and expertise for the lithogeochemical and geochronological component of this study. We also thank Alan Galley for a review and helpful comments.

REFERENCES

Ayer, J., Amelin, Y., Corfu, F., Kamo, S., Ketchum, J., Kwok, K., and Trowell, N., 2002. Evolution of the southern Abitibi greenstone belt based on U-Pb geochronology: autochthonous volcanic construction followed by plutonism, regional deformation and sedimentation; Precambrian Research, v. 115, p. 63–95.

Ayer, J.A. and Chartrand, J.E., 2011. Geological compilation of the Abitibi greenstone belt; Ontario Geological Survey, Miscellaneous Release Data 282.

Barker, F., 1979. Trondhjemites, Dacites and Related Rocks; Elsevier, New York, 659 p.

Berger, B.R., 2011. Geological investigations south of Gogama, In: Summary of Field Work and Other Activities 2011; Ontario Geological Survey, Open File Report 6270, 7 p.

Berger, B.R., 2012. Interpretation of Geochemistry in the south of Gogama area, In: Summary of Field Work and Other Activities 2012; Ontario Geological Survey, Open File Report 6280, 14 p.

Campbell, I.H., Franklin, J.M., Gorton, M.P., Hart, T.R., and Scott, S.D., 1981. The role of subvolcanic sills in the generation of massive sulfide deposits; Economic Geology, v. 76, p. 2248–2253.

Dubé, B. and Gosselin, P., 2007. Greenstone-hosted quartz-carbonate vein deposits, *In:* Mineral Deposits of Canada: A Synthesis of Major Deposit Types, District Metallogeny, the Evolution of Geological Provinces, and Exploration Methods, (ed.) W.D. Goodfellow; Geological Association of Canada, Mineral Deposits Division, Special Publication No. 5, p. 49–73.

Galley, A.G., 2003. Composite synvolcanic intrusions associated with Precambrian VMS-related hydrothermal systems; Mineralium Deposita, v. 38, p. 443–473.

Galley, A.G. and Lafrance, B., 2014. Setting and evolution of the Archean synvolcanic Mooshla Intrusive Complex, Doyon-Bousquet-LaRonde mining camp, Abitibi greenstone belt: Emplacement history, petrogenesis, and implications for Au metallogenesis; Economic Geology, v. 109, p. 205–229.

Heather, K.B. and van Breemen, O., 1994. An interim report on geological, structural, and geochronological investigations of granitoid rocks in the vicinity of the Swayze greenstone belt, southern Superior Province, Ontario, *In:* Canadian Shield; Geological Survey of Canada, Current Research 1994-C, p. 259–268.

Heather, K.B., Shore, G.T., and van Breemen, O., 1996, Geological investigations in the Swayze greenstone belt, southern Superior Province, Ontario: a final update, *In:* Canadian Shield; Geological Survey of Canada, Current Research 1996-C, p. 125–136.

Heather, K.B. and Shore, G.T., 1999a. Geology, Swayze Greenstone Belt, Ontario; Geological Survey of Canada, Open File 3384a, sheet 2, scale 1:50 000.

Heather, K.B. and Shore, G.T., 1999b. Geology, Gogama, Swayze Greenstone Belt, Ontario; Geological Survey of Canada, Open File 3384g, scale 1:50 000.

Heather, K.B., 2001. The geological evolution of the Archean Swayze Greenstone Belt, Superior Province, Canada; Ph.D. thesis, Keele University, Keele, England, 370 p.

IAMGOLD Corporation, 2013. IAMGOLD provides mineral resource update for Côté Gold and reports strongest quarter for production in 2012 with confirmed production guidance for 2013; IMG press release, January 22, 2013.

Kontak, D.J., Creaser, R.A., and Hamilton, M., 2013. Geological and geochemical studies of the Côté Lake Au(-Cu) deposit Area, Chester Township, Northern Ontario, *In:* Results from the Shining Tree, Chester Township and Matachewan Gold Projects and the Northern Cobalt Embayment Polymetallic Vein Project, (ed.) J.A. Ayer, D.J. Kontak, R.L. Linnen, and S. Lin; Ontario Geological Survey, Miscellaneous Release Data 294.

Lesher, C.M., Goodwin, A.M., Campbell, I.H., and Gorton, M.P., 1986. Trace-element geochemistry of ore-associated and barren, felsic metavolcanic rocks in the Superior Province, Canada; Canadian Journal of Earth Sciences, v. 23, p. 222–237.

Poulsen, K.H. and Franklin, J.M., 1981. Copper and gold mineralization in an Archean trondhjemitic intrusions, Sturgeon Lake, Ontario; Geological Survey of Canada, Paper 81-1a, p. 9–14.

Poulsen, K.H., Robert, F., and Dubé, B., 2000. Geological classification of Canadian gold deposits; Geological Survey of Canada, Bulletin 540, 106 p.

Powell, W.G., Carmichael, D.M., and Hodgson, C.J., 1995. Conditions and timing of metamorphism in the southern Abitibi greenstone belt, Québec; Canadian Journal of Earth Sciences, v. 32, p. 787–805.

Robert, F., 2001. Syenite-associated disseminated gold deposits in the Abitibi greenstone belt, Canada; Mineralium Deposita, v. 36, p. 503–516.

Robert, F., Poulsen, K.H., Cassidy, K.F., and Hodgson C.J., 2005. Gold metallogeny of the Yilgarn and Superior cratons, *In:* Economic Geology 100th Anniversary Volume: 1905–2005, (ed.) J.W. Hedenquist, J.F.H. Thompson, R.J. Goldfarb, and J.P. Richards; Society of Economic Geologists, Littleton, Colorado, p. 1001–1034.

Sun, S.S. and McDonough, W.F., 1989. Chemical and isotopic systematics of ocean basalts: Implications for mantle composition and process, *In:* Magmatism and Ocean Basins, (ed.) A.D. Saunders and M.J. Norry; Geological Society of London, p. 313–345.

Trowell, N.F., 1974. Geology of the Bell Lake-Sturgeon Lake area, districts of Thunder Bay and Kenora; Ontario Geological Survey, Report 113, 67 p.

Van Breemen, O., Heather, K.B., and Ayer, J.A., 2006. U-Pb geochronology of the Neoarchean Swayze sector of the southern Abitibi greenstone belt; Geological Survey of Canada, Current Research 2006-F1, 32 p.

Winchester, J.A. and Floyd, P.A., 1975. Geochemical magma type discrimination: Application to altered and metamorphosed basic igneous rocks; Earth and Planetary Science Letters, v. 28, p. 459–469.